Journal of Alloys and Compounds 910 (2022) 164868

Contents lists available at ScienceDirect

Journal of Alloys and Compounds

journal homepage: www.elsevier.com/locate/jalcom

High-throughput evaluation of stress–strain relationships in Ni–Co–Cr ternary systems via indentation testing of diffusion couples

Kenta Goto[a], Ayako Ikeda[b], Toshio Osada[b,*], Ikumu Watanabe[b], Kyoko Kawagishi[b], Takahito Ohmura[b]

[a] International Center for Young Scientists, National Institute for Materials Science, 1-2-1 Sengen, Tsukuba 305-0047, Japan
[b] Research Center for Structural Materials, National Institute for Materials Science, 1-2-1 Sengen, Tsukuba 305-0047, Japan

ARTICLE INFO

Article history:
Received 12 January 2022
Received in revised form 1 April 2022
Accepted 1 April 2022
Available online 4 April 2022

Keywords:
Combinatorial experiment
Nanoindentation
Nickel-based superalloy
Elastoplastic deformation
Solid solution hardening

ABSTRACT

The experimental investigations of multi-component alloy systems require considerable time and effort in terms of sample preparation; in particular, when studying numerous material compositions, the melting, processing, and machining of each specimen at each composition are significantly time- and effort-intensive. To overcome this challenge, the high-throughput evaluation of the stress–strain curves associated with the chemical compositions and microstructures of a Ni–Co–Cr ternary system was performed by estimating the yield stress and tangent modulus via indentation testing. Four diffusion couples (involving the diffusion of Ni and Co) with different nominal Cr contents were prepared, and more than 570 stress-strain curves at the points with different chemical compositions and microstructures were measured. The addition of Cr solute increased the elastic modulus and hardness and decreased the normalized pile-up height, indicating a low strain hardening behavior. The estimated yield stress was strongly dependent on the Cr content, whereas the Co content did not sufficiently affect the strength. Moreover, the effects of crystal orientation on the indentation testing of the face-centered cubic and hexagonal close-packed phases are discussed. The proposed technique can facilitate the evaluation of elastoplastic behavior in multi-component systems in single phase (fcc), which can help achieve the statistical data-driven material development of Ni-based superalloys.

1. Introduction

Ni-based superalloys exhibit satisfactory mechanical properties at high temperatures and are thus widely used in jet engines. These materials can be strengthened through hierarchical mechanisms, specifically by the utilization of grain and twin boundaries, precipitation of the γ' phase, and use of additive elements [1,2]. To maximize the strengthening effect, Ni-based superalloys contain more than 10 elements. For example, the γ phase in the U720Li alloy contains 20 wt% of Co, 27 wt% of Cr, and at least four other elements, such as molybdenum and tungsten [3]. Consequently, it is desirable to elucidate the contribution of the additive elements to the strength, so the alloy composition can be optimized. Notably, the experimental investigations of multi-component systems require considerable time and effort in terms of sample preparation; in particular, when studying numerous material compositions, the melting, processing, and machining of each specimen at each composition are significantly time- and effort-intensive. To overcome these challenges, a numerical approach using first-principle calculations has been established; however, the number of possible additive elements remains limited [4,5].

A combinatorial approach using a composition gradient sample and nanoindentation technique can facilitate the high-throughput evaluation of the effects of additive elements on the intragranular strength. Nanoindentation techniques have been widely used to investigate the mechanical responses in small regions within a grain interior of sample with fine microstructures. Through the formation of local deformations in a target sample, the mechanical properties at various compositions of a composition gradient sample can be identified. Samples for nanoindentation can be fabricated using several methods, such as the diffusion multiple technique [6–9], Bridgeman method [10], mechanical stirring [11,12] and three-dimensional (3D) printing [13,14]. Kadambi et al. [7] investigated the change in hardness (H) with the composition of six binary alloys, such as Ni–Co and Ni–Fe, using diffusion couples and performing nanoindentation testing. Assuming that the hardness is proportional

* Corresponding author.
E-mail address: OSADA.Toshio@nims.go.jp (T. Osada).

https://doi.org/10.1016/j.jallcom.2022.164868
0925-8388/

to the yield stress (σ_Y) [15], that is, $H = C_T\sigma_Y$, the authors demonstrated that the Labusch relationship [16] holds for H of these binary alloy systems. Combinatorial nanoindentation testing has also been used for the screening of high-entropy alloys in several studies [17,18].

Notably, although the aforementioned relationship between the H and σ_Y is widely accepted, the proportionality coefficient, C_T, depends on the material species. Tabor [19] introduced the concept of a representative stress (σ_R) at a representative strain (ε_R) ≈ 8% corresponding to the deformed plastic zone induced by indentation. Moreover, the assessment of the stress–strain curves as well as the strain-hardening behavior in the local region is critical for realizing numerical simulations, such as those pertaining to the nonlinear finite element analyses of heterogeneous materials [20]. Various techniques have been developed to estimate the stress–strain relationships based on indentation results [21–23]. In a previous study [24,25] the authors attempted to determine these plastic properties by performing a Berkovich indentation test and evaluating the pile-up height in the vicinity of an indent and the H value. No study has yet been reported on the application of estimation techniques to the indentation combinatorial approach, enabling the high-throughput evaluation of the stress–strain curve.

Our previous study using Bridgeman method [10] shows that the combinatorial nanoindentation testing is also useful for understanding to phase stability, oxidation resistance, and hardness in advanced Ni-based superalloy with γ-γ' two phase structure. Meanwhile, in order to clear understanding the hieratical strengthening mechanisms and predict a total strength in Ni-based superalloy including both solid solution and γ' precipitation strengthening, the data only for solid-solution strengthening is also important [2,3]. Thus, this study aimed to evaluate σ_Y and the tangent modulus (B) by a high-throughput evaluation through the indentation testing on the composition gradient samples of a Ni–Co–Cr ternary alloy as an example of fundamental elements for the γ formers in Ni-based superalloys.

2. Experimental

Four diffusion couples, including Ni, Co, and Cr, were prepared (Table 1) with different nominal Cr contents (c_{Cr}) of 0, 7, 14, and 20 at %. First, four pairs of Ni–Cr and Co–Cr binary alloys with the same c_{Cr} were prepared by arc melting. The pairs, cut into plates with dimensions of 10 × 10 × 1 mm^3, were alternately stacked and bonded by spark plasma sintering at 10 MPa and 700 °C for 5 min in vacuum. Thereafter, the specimens were subjected to heat treatment at 1150 °C for 3000 h to diffuse the Ni and Co elements, followed by hot isostatic pressing (HIP) at 1120 °C under 98 MPa for 4 h to eliminate voids. A thermodynamic calculation software (ThermoCalc [26]) with the TCNI9 database showed that all the compositions considered in this study (Ni–Co–Cr for c_{Cr} < 20 at%) exhibit the face-centered cubic (fcc) single phase at 1120 and 1150 °C. Next, the diffusion couples were cut and mechanically polished. The polishing was completed by conducting vibration polishing to remove any residual strain induced by mechanical polishing.

Table 1
Diffusion couples used in this study.

	Nominal c_{Cr} [at%]	Number of rows and columns for indentation
Sample A	0	11 × 14
Sample B	7	3 × 51
Sample C	14	11 × 14
Sample D	20	11 × 11

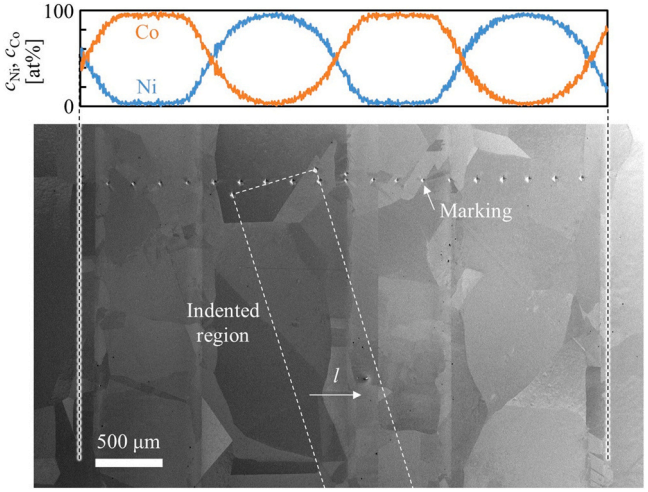

Fig. 1. Secondary electron image of the diffusion couple and profiles of c_{Ni} and c_{Co} measured using EDS for Sample A.

Fig. 1 shows a field-emission scanning electron microscopy (FESEM; EISS Gemini SEM 300, Germany) image of a Ni–Co binary diffusion couple (Sample A) after polishing. Energy-dispersive X-ray spectroscopy (EDS) measurements indicated that the Ni and Co contents (c_{Ni} and c_{Co}, respectively) changed continuously around the contact surfaces of the plates along the stacking direction (l). Nanoindentation was performed using a Triboindenter TI950 (Bruker) instrument and a diamond Berkovich indenter in the region surrounded by the white dotted line. In some samples, small Kirkendall voids still remain despite the HIP treatment. In order to avoid voids, the number of rows and columns for indentation was adjusted as shown in Table 1.

The maximum load, loading rate, and holding time were 10 mN, 1 mN/s, and 10 s, respectively. The reduced elastic modulus E_r and indentation H were determined from a load–displacement curve during an unloading step using the Oliver–Pharr method [27]. After each indentation, the 3D topography of the residual indentation mark was acquired by atomic force microscopy (AFM); the atomic force microscope was incorporated into the TI950 instrument. The maximum pile-up height (h_p) was calculated from a cross section across a vertex and the center of the side of the indentation mark at each side. The normalized pile-up height (H_p) was obtained as follows:

$$H_p = \left(\sum_{k=1}^{3} h_{p(k)}\right)/h_{max}. \quad (1)$$

The indented region was analyzed using an electron probe microanalyzer (EPMA; EPMA-8050 G, Shimadzu), and the electron backscatter diffraction (EBSD) measurements were obtained using Auriga (Carl Zeiss).

3. Results

3.1. Ni–Co binary system

Before examining the ternary system, the results of Sample A were considered. Fig. 2a shows an optical image of the indented region shown in Fig. 1. The indentation was performed in a matrix shape involving 11 rows and 14 columns inclined against l. The indentation interval in each row is 200 μm. Hintsala et al. [28] demonstrated that an indentation was affected by its neighboring indent when the interval was less than the contact radius by a factor

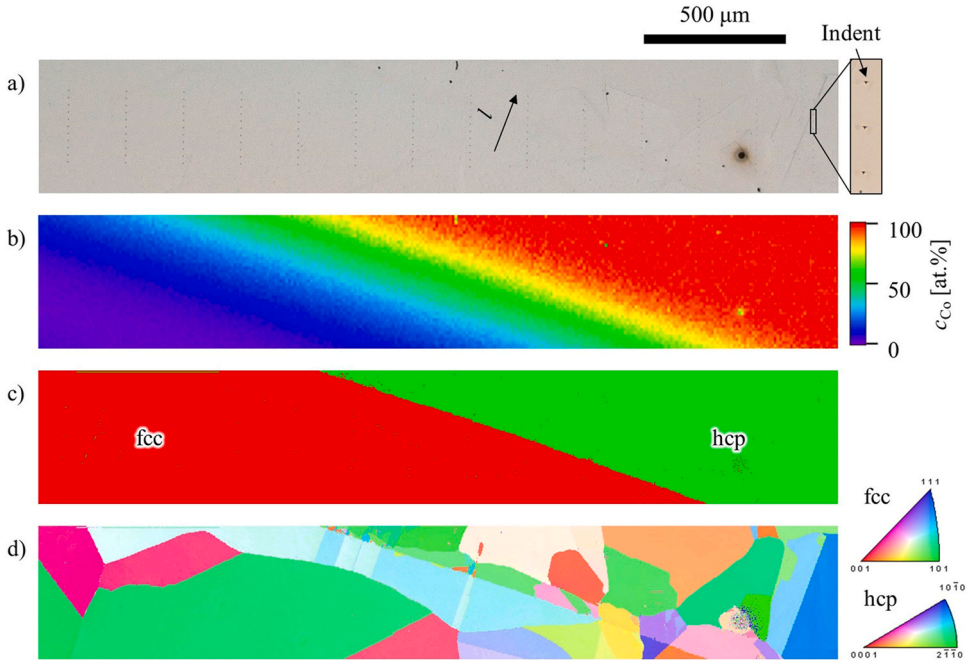

Fig. 2. a) Optical image and maps of b) c_{Co}, c) phase, and d) IPF at the indented region shown in Fig. 1.

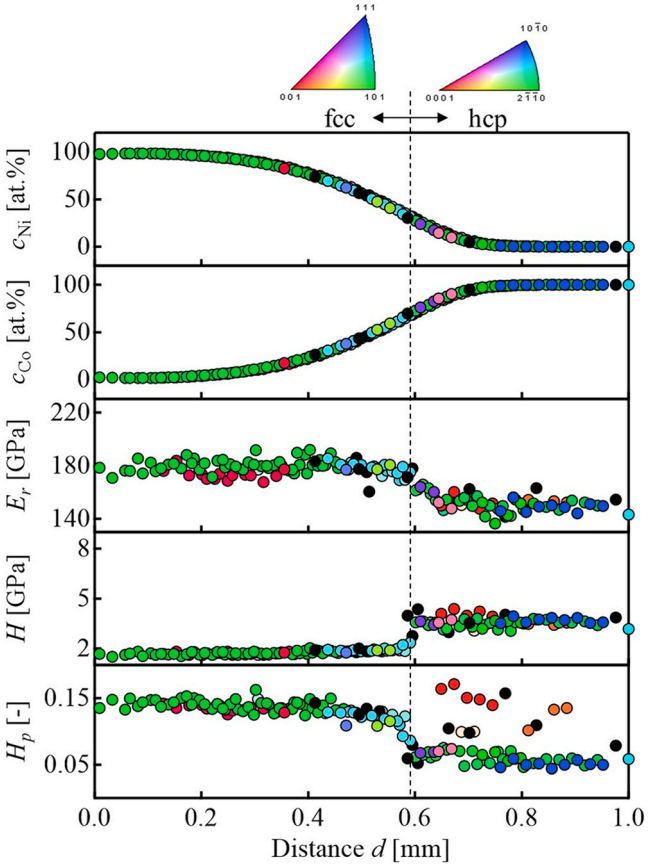

Fig. 3. Distributions of c_{Ni} and c_{Co}, reduced E_r, H, and H_p in Sample A. Each spot is colored in accordance with the IPF map, and the black spots represent the indentation on the grain boundaries.

of 5.6. In this study, the contact radius and h_{max} were less than 2 µm and 500 nm, respectively, indicating that the interval was sufficiently large to ignore the effects of the neighboring indents. Additionally, the interval can be decreased depending on the desired resolution in the element content, but it should be balanced with a testing time. The c_{Co} map (Fig. 2b) shows that the left region is Ni-rich, and c_{Co} increases toward the right side. The Ni-rich region exhibited an fcc structure, whereas a hexagonal close-packed (hcp) structure was observed at $c_{Co} > 70$ at% (Fig. 2c). Pure Co undergoes martensitic transformation from fcc to hcp at ~420 °C, and the transformation temperature decreases as the c_{Ni} increases [29]. The transformation is rapid in that the hcp phase is observed even after water quenching in $Co_{90}Ni_{2.5}Cr_{2.5}Fe_{2.5}Mn_{2.5}$ [30]. Therefore, in this study, the hcp phase likely appeared during furnace cooling after HIP. The sample is polycrystalline, as shown in the inverse pole figure (IPF) map (Fig. 2d). The effects of the crystal orientation are discussed later. Fig. 3 shows the variation in the contents and indentation results with the distance (d) from an indent at the side along l. c_{Ni} decreases and c_{Co} increases monotonically as d increases. E_r and H, obtained from the indentation load–displacement curves, and H_p, calculated from the AFM results marginally changed with d in the fcc and hcp phases, although significant changes were observed at the phase boundary.

According to the EPMA and indentation results, the variations of E_r and H with c_{Co} are plotted, as shown in Fig. 4. E_r is constant at ~180 GPa for $c_{Co} < 40$ at%, and a significant drop in E_r is observed for $c_{Co} = 70$–80 at% in the hcp phase. Yang et al. [5] demonstrated that the Young's modulus increased by 3% as c_{Co} increased from 5 to 30 at %; however, such a slight change could not be observed owing to the standard error in the nanoindentation technique. For example, the standard error was 4.8% for $c_{Co} < 5$ at%. It is possible that the decrease in E_r at $c_{Co} > 40$ at% was caused by the small Kirkendall voids remaining in the microstructure as expected from several large voids observed around the phase boundary on the hcp side although HIP was performed after diffusion annealing. H increased slightly with d

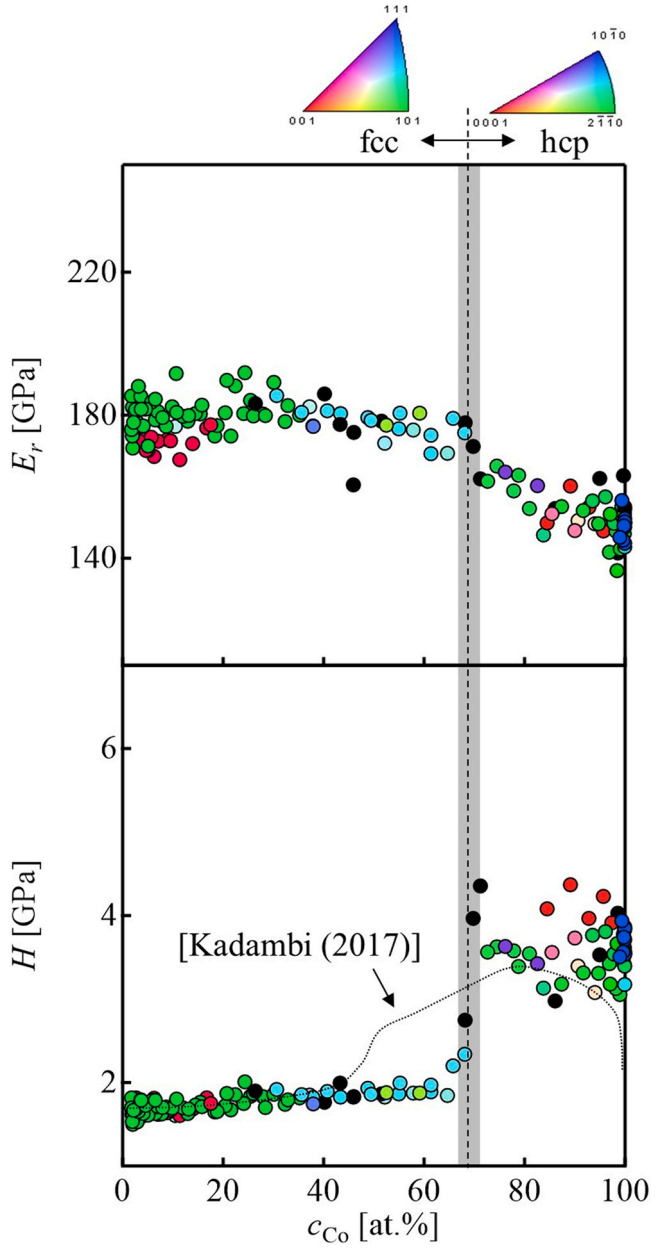

Fig. 4. Variations in E_r and H with c_{Co} for Sample A. Each spot is colored in accordance with the IPF map, and the black spots represent the indentations on the grain boundaries. Spots in the gray band represent indents with deformed regions across both phases.

and increased from ~2.0 to ~3.5 GPa near the phase boundary. The results reported by Kadambi et al. [7], who performed indentation on a Ni–Co diffusion couple, were in agreement with our results, except for those at c_{Co} = 40–70 at%, as indicated by a dotted line in Fig. 4. Specifically, at c_{Co} = 40–70 at%, the H obtained in this study was lower than that reported previously [7], likely because of the different maximum indentation loads (10 mN in this study and 20 mN in [7]) and composition gradient distances.

In indentation combinatorial testing using polycrystalline samples, the effects of the crystal orientation on the indentation result must be examined to evaluate the solid solution effect. Each point in Figs. 4 and 5 is colored according to the crystal orientation as well as the IPF map (Fig. 2d), with the black spots representing the indentations on the grain boundaries. In terms of the crystal orientation dependence of E_r at c_{Co} < 20 at%, the indentations on the (001) plane returns lower E_r values than those on the (101) plane. H on (001) is comparable to that of (101) in the fcc phase. This tendency agrees with those observed in previous experimental and theoretical studies [31,32]. Among the examined samples, the fcc alloy exhibited the highest and lowest E_r on the (111) and (001) planes, respectively, although H was virtually independent of the orientation. Moreover, E_r did not depend on the orientation in the hcp phase, and H was larger on the (0001) plane than on the other planes. In the indentation testing of titanium, which exhibited an hcp structure, the highest H was observed on the (0001) plane [33] owing to the limited slip of the basal plane parallel to the surface.

Fig. 5 shows the variation of H_p with c_{Co}. Specifically, H_p is ~0.14 at c_{Co} = ~0 at% and continuously decreases with c_{Co}. Following the large drop at the phase boundary, H_p increases slightly in the c_{Co} range of 70–100 at%. The crystal orientation dependence is similar to that of H, that is, relatively low in fcc and high in hcp configurations. H_p on (0001) is larger than that on ($10\bar{1}0$) by a factor of three. Fig. 5 shows the AFM gradient images of the indents on (0001) and ($10\bar{1}0$). The (0001) indent exhibits pileups at all the edges. In contrast, the ($10\bar{1}0$) indent exhibits small pileups at the two edges on the right and no pile-ups on the left side and is in agreement with the results for titanium [33].

3.2. Ni–Co–Cr ternary system

Fig. 6 shows the optical image and EPMA and EBSD results of Sample C, and the variations in the contents and indentation results with d along l are plotted in Fig. 7. c_{Ni} decreases and c_{Co} increases with increasing d, as in the case of Sample A. The average c_{Cr} was 14.1 at% albeit with an inhomogeneous distribution owing to the different chemical potentials of Cr in Ni and Co. The maximum and minimum c_{Cr} were 15.0 and 13.3 at% in the Ni-rich region and near the phase boundary, respectively. Beyond d = 0.46 mm, the phase changed from the fcc phase to the fcc + hcp dual phase. The grains in the dual phase were finer than those in the hcp phase in Sample A; consequently, several indents are located on the grain boundaries. The changes in E_r, H, and H_p were larger at the phase boundary than those within the phases. The large variation in the dual phase is attributable to the crystal orientation and grain boundaries. The results for samples B and D are shown in the Supplementary material.

The results of four samples with different nominal c_{Cr} are plotted in ternary diagrams, as shown in Fig. 8. Each measurement point is represented by a circle, and the areas among the plots are interpolated using the natural neighbor interpolation method. The fcc and hcp phases are observed at the low c_{Co} and high c_{Ni}, respectively. The fcc + hcp dual phase was observed at the high c_{Co} and c_{Cr}. The presented phase diagram is *not* in equilibrium; however, a stable phase is achieved after slow cooling from 1120 °C. The indentation results are indicated by the shapes of the ternary diagrams (the region surrounded by green lines in the phase map). E_r is approximately constant at ~180 GPa. The addition of 20 at% Cr to Ni increases E_r by 10 GPa, which is consistent with previous studies [34]. H is higher in the hcp and dual phases than in the fcc phase. H_p exhibited large variations in the hcp and dual phases and is lower than that in the fcc phase. Magnified views of the ternary diagrams, including only the fcc region at c_{Co} < 50 at%, are shown on the left side (region surrounded by orange lines). The addition of Cr significantly increased E_r and H and decreased H_p in the fcc region.

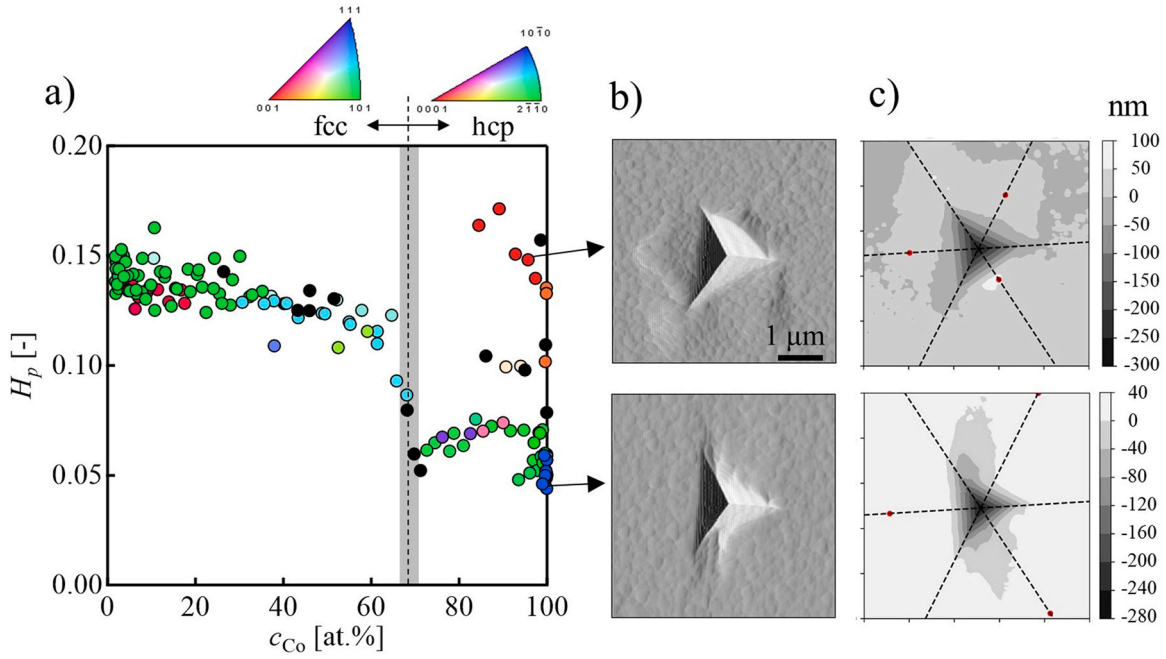

Fig. 5. a) Variations in H_p with c_{Co} for Sample A with the AFM maps at $c_{Co} \approx 100$ at% showing high and low H_p values. Each spot is colored in accordance with the IPF map, and the black spots represent the indentations on the grain boundaries. Spots in the gray band represent indents with deformed regions across both phases; b) gradient images; c) maximum height points (marked as red points) on contour map of measured height from topography images which removed the tilt by considering the entire image.

3.3. High-throughput estimation of the stress–strain relationship

A stress–strain curve, including σ_Y and the strain hardening data, is more important than the H data. In this section, the estimation of the stress–strain relationship is adopted for the combinatorial indentation tests.

Assuming a linear hardening law for the stress–strain curve of Ni alloys (see Supplementary material), the elastoplastic behavior can be represented as Eq. (2):

$$\sigma = E\varepsilon \ at \ \sigma \le \sigma_Y; \sigma = A + B\varepsilon \ at \ \sigma > \sigma_Y, \tag{2}$$

where σ, ε, E, A, and B denote the stress, strain, Young's modulus, intercept, and tangent modulus, respectively. Here, $\sigma_Y = \frac{A}{(1-B/E)}$. Based on Tabor's theory [19], σ_R is proportional to the H, that is, with a constant k_e,

$$H = k_e \sigma_R \tag{3}$$

ε_R, returning σ_R, is approximately 8% ($\sigma_R = \sigma_0 + B\varepsilon_R$). The H_p also involves information on the hardening behavior. The H_p value should be 0 in an elastic material ($\sigma_Y/E = \infty$ or $B/E = 1$) and maximum in the perfect plastic deformation ($\sigma_Y/E = 0$ or $B/E = 0$) [35]. According to [25], the relationship of H_p with σ_Y and B was approximated by

$$H_p = k_{p1}\exp\left\{-k_{p2}\left(\frac{\sigma_Y}{E_{rs}}\right) - k_{p3}\left(\frac{B}{E_{rs}}\right)\right\}. \tag{4}$$

Here, instead of E, E_{rs}, which is the indentation modulus, is used which is defined as follows:

$$\frac{1}{E_r} = \frac{1-\nu_i^2}{E_i} + \frac{1}{E_{rs}}, \tag{5}$$

where E_i and ν_i denote the Young's modulus and Poisson's ratio of the indenter, respectively; $E_i = 1140$ GPa and $\nu_i = 0.07$ for diamond. The fitting parameters k, k_{p1}, k_{p2}, and k_{p3} were determined as listed in Table 2 from the results of uniaxial tensile tests and indentation testing at a maximum load of 10 mN considering the Ni alloy and stainless steel to ignore the indentation size effects [36]. The validity of the determined fitting parameters and the assumption of linear hardening law can be seen in the stress-strain curves in Supplementary Fig. S5. The true stress-true strain curves obtained by the inversed analysis for pure Ni, Ni-20at%Co-10at%Cr and Ni-40at%Co-20at%Cr are in good agreement with those obtained by conventional tensile tests. Here, fitting parameters were determined using curves below 10% strain in order to improve the prediction accuracy of yield stress and work hardening factors around it, which are important as an alloy properties data. Further, it should be noted that, only two fitting parameters can be estimated using the method, and Ludwigson and swift laws involving three or more plasticity parameters cannot be inverse analyzed.

Based on Eqs. (2)–(5), σ_Y and B can be determined from the indentation results of E_r, H, and H_p. The plastic parameters in the Ni–Co–Cr ternary system were estimated in the fcc phase for $c_{Co} < 50$ at%, as the crystal orientation dependence was high in the hcp structure.

The estimated σ_Y exhibited a strong dependence on c_{Cr} (Fig. 9a). The addition of 20 at% Cr increases σ_Y by a factor of three, whereas the addition of Co is less effective for strengthening. Although B (Fig. 9b) shows a similar variation trend as σ_Y, the change in B is relatively small; its value is higher by a factor of 1.2 in Ni-40 at%Co-20 at%Cr than in Ni. Fig. 9c shows the stress–strain curves based on Eqs. (2) for the four compositions shown in Fig. 9a. The estimated stress at $\varepsilon = 10\%$ is 255.4 MPa in Ni. The addition of 40 at% Co and 20 at% Cr increased the stress by 21.9 and 222.7 MPa, respectively. When 40 at% Co and 20 at% Cr are added, the stress increases by 258.0 MPa. Yang et al. [5] demonstrated the strong dependence of Cr on the strength of Ni–Co–Cr systems using first-principle calculations, and the findings are in agreement with the obtained results. Meanwhile, it is important to mention error of estimated σ_Y from the

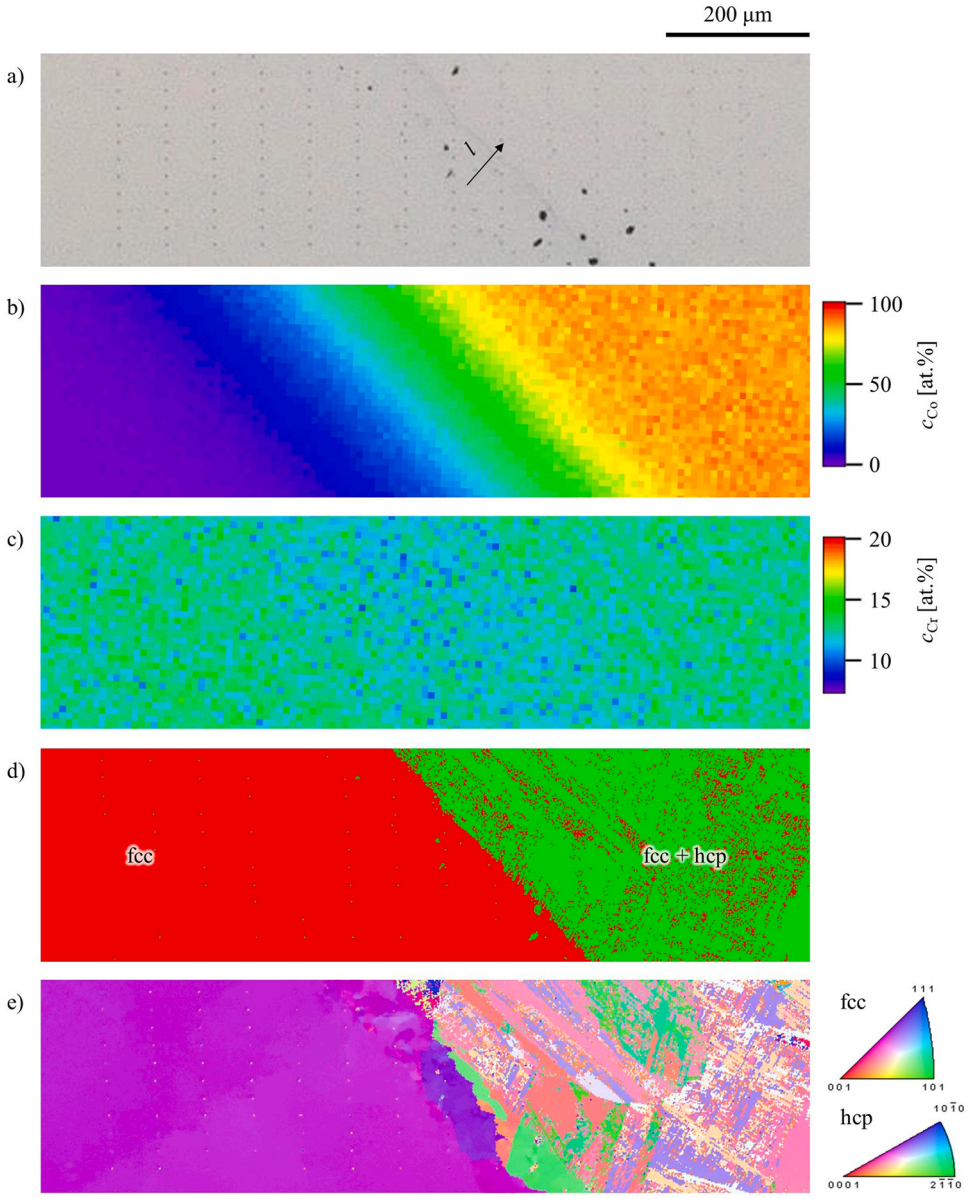

Fig. 6. a) Optical image and maps of b) c_{Co}, c) c_{Cr}, d) phase, and e) IPF in the indented region for Sample C.

measured E_r, since the E_r is well known to have a relatively large variability. As shown in Fig. 4, accuracy of E_r measured was around ± 10 GPa. The accuracy of estimated σ_Y corresponding to the values is ± 6.9 MPa, indicating to that our method has sufficient prediction accuracy.

4. Discussion

Our proposed technique enables the high-throughput experimental evaluation of σ_Y and the strain-hardening behavior. For example, in the present test, more than 570 points of mechanical properties were automatically obtained for Ni-Co-Cr ternary diffusion materials with different compositions, and the time required for the indentation tests was only 28.5 h. On the other hand, to conduct a tensile test using the conventional method with the same number of points, the total time required for specimen machining, including electrical discharge machining, rough cutting, grinding, and several types of polishing, as well as the room temperature tensile tests, would require approximately 200 days. Therefore, the proposed high-throughput evaluation method is 168 times faster than the conventional test method, although it is only a rough estimation. Furthermore, in order to actually conduct tensile tests on 570 types of multi-component alloys, casting, forging and heat treatment must be conducted under optimal conditions for each composition. Since process optimization is a trial-and-error process, the effect of high throughput is expected to be even greater than 168 times.

Further, the huge amount of experimental data set of hardness and Young's modulus linked to crystal orientation could be useful for understanding to the orientation dependent. Our results indicate that crystal orientation dependent of H and H_p in hcp are significantly larger than those in fcc for all the gradient samples as shown in Figs. 4 and 5. Since the deviation in hcp phase does not depend on the Co content, the variety is attributed to the hcp crystal structure with the higher anisotropy of plasticity. Additionally, the

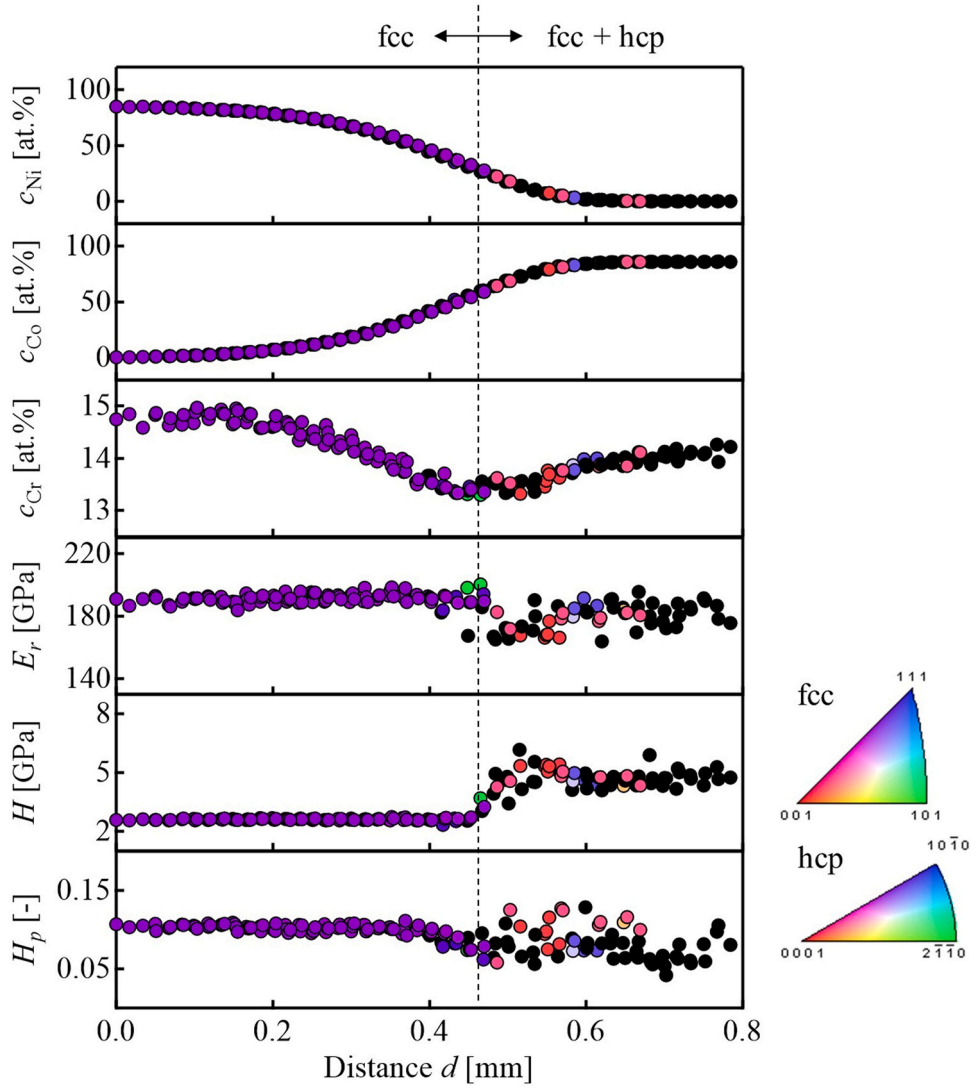

Fig. 7. Distributions of c_{Ni}, c_{Co}, c_{Cr}, E_r, H, and H_p in the Ni–Co–Cr ternary diffusion couple (Sample C). Each spot is colored in accordance with the IPF map, and the black spots represent the indentations on the grain boundaries.

higher hardness H in hcp phase close to {0001} orientation with red marks in Fig. 4 corresponds well to the higher strain hardening in the same red marks in Fig. 5, indicating that the higher hardness is originated from the higher strain hardening. When Berkovich indenter is induced in the direction normal to basal plane, the resolved shear stress (RSS) on the basal is significantly small and hence the non-basal slip systems must be also activated to accommodate to the induced plastic strain. Therefore, multi slip systems were presumably activated underneath the indenter, leading to the higher strain hardening. Meanwhile, E_r and H_p values show a certain orientation dependence even for the fcc structure. In this study, we ignored the orientation dependence for E_r and H_p in fcc for σ_Y estimation, because of its small orientation dependence, but the analysis of the dependence will be important for further improved accuracy of σ_Y estimation, as a future work.

The method could contribute the evaluation of the solid solution strengthening effect on the strain-hardening behavior in multi-component systems. The conventional theory for σ_Y in multi-component systems was proposed by Gypen and Deruyttere [37], in which an increase in the critical resolved shear stress could be expressed as the sum of each increment by a solute element, assuming no interactions between different elements. Varvenne et al. [38] proposed a more sophisticated theory for high-entropy alloys. These theories are based on Labusch's theory for binary alloys [16,39] and enable the estimation of σ_Y from size and elastic misfits.

The theory of strain hardening has not yet been established and remains controversial. In general, strain-hardening behavior depends on the stacking fault energy (SFE). A low SFE causes a large strain hardening, as the increase in the stacking fault width caused by the low SFE prevents the occurrence of cross-slip and subsequent dynamic recovery. The SFE decreases with an increase in the c_{Co} and c_{Cr} in Ni–Co and Ni–Cr binary alloys [40,41], which is representative of an increment in the flow stress during strain hardening with increasing c_{Co} and c_{Cr}. This result agrees with the experimental results shown in Fig. 9c. Contrary to that for σ_Y, no theory has been established regarding the effects of the solid solution on the strain-

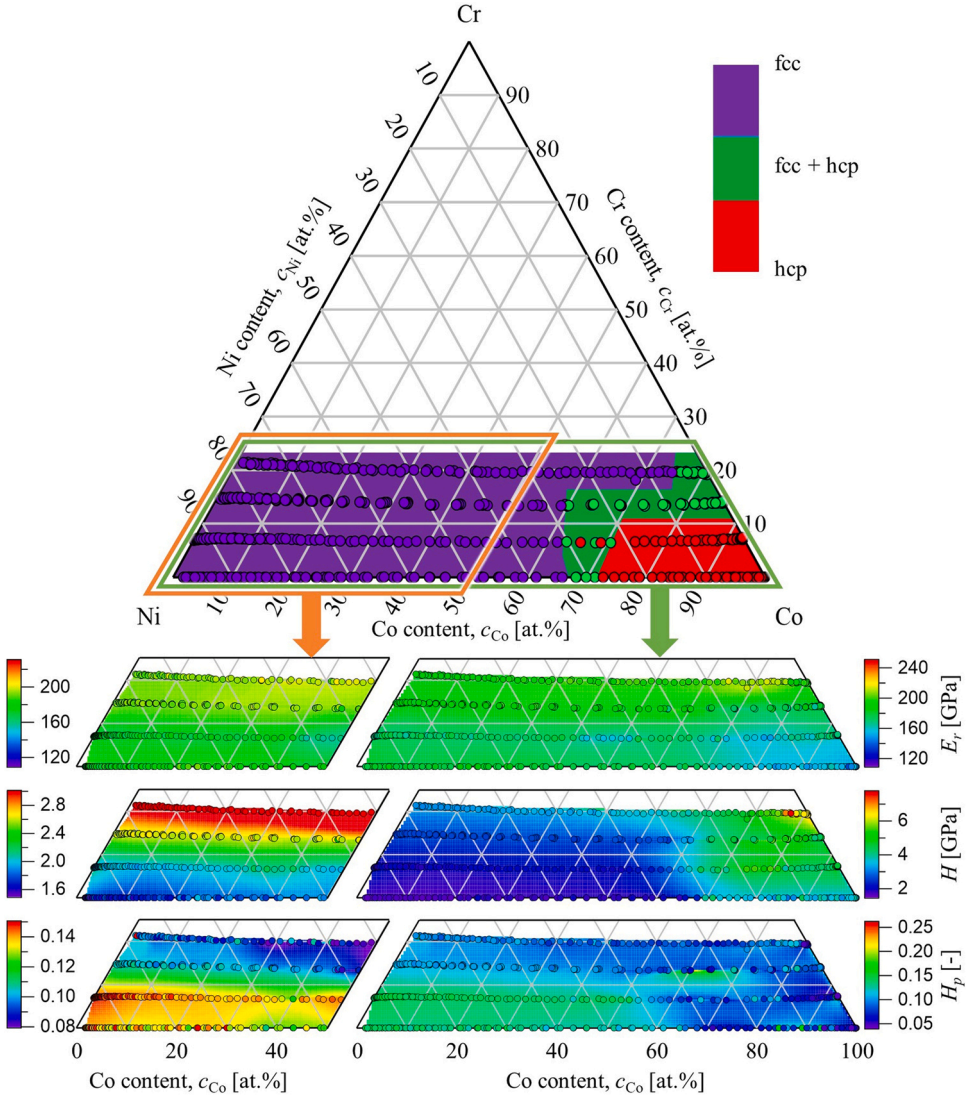

Fig. 8. Ternary diagrams for the phase, E_r, H, and H_p. Each spot represents a measurement point. Phase diagram exhibits stable phases after slow cooling from 1120 °C.

Table 2
Fitting parameters used to estimate σ_Y and B.

Parameter	k_e	k_{p1}	k_{p2}	k_{p3}
Value	7.23	0	0	229.1

hardening exponent. The tool proposed in this study can enable the comprehensive evaluation of the solid solution strengthening effect on the strain-hardening behavior in multi-component systems, including superalloy and high-entropy alloy with more than 10 additive elements.

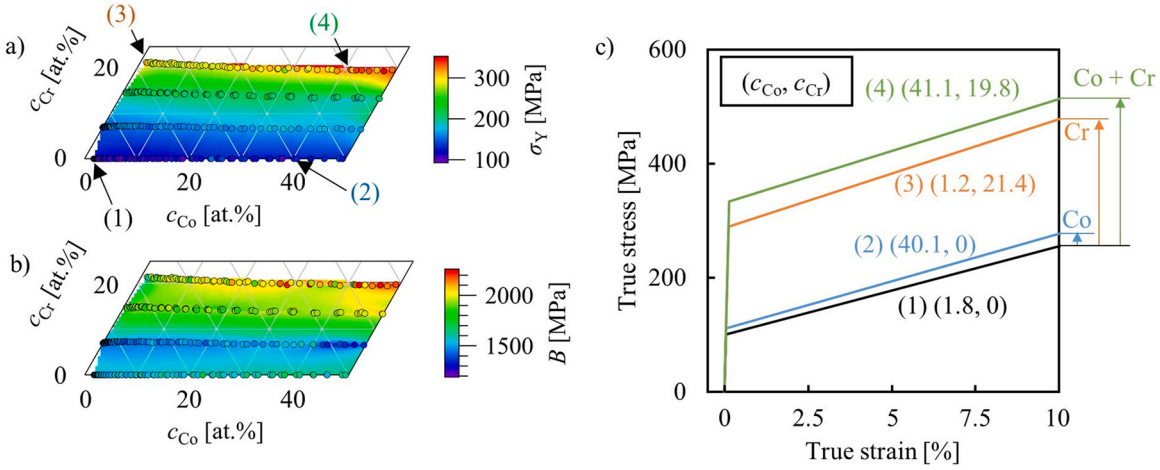

Fig. 9. Ternary diagrams for estimated (a) σ_Y, (b) strain-hardening exponent at c_{Co} < 50 at%, and (c) estimated stress–strain curves at (c_{Co}, c_{Cr}) = (1.8, 0), (40.1, 0), (1.2, 21.4), and (41.1, 19.8) at%.

5. Conclusions

The high-throughput evaluation of the stress–strain relationship in a Ni–Co–Cr ternary system was performed via the indentation testing of diffusion couples and estimation of the uniaxial plastic properties. The following conclusions were drawn.

(1) More than 570 stress-strain curves for various chemical compositions were obtained from four diffusion couples by using inverse estimation approach from load–displacement curves during nanoindentation tests.
(2) The proposed high-throughput evaluation method is approximately > 168 times faster than the conventional test method, including electrical discharge machining, rough cutting, grinding, several types of polishing, and the room temperature tensile tests.
(3) The addition of Cr had a more significant effect on the mechanical properties than by that of Co, in accordance with previously reported results. E_r and H increased with increasing c_{Cr}; however, H_p decreased.
(4) The Ni-rich fcc phase returned a smaller E_r on the (001) plane than on the (101) plane; however, H and H_p were independent of the crystal orientation. In contrast, the hcp crystal in the Co-rich composition exhibited high H and H_p values on the (0001) plane owing to the suppression of the basal slip.
(5) The estimation of σ_Y and B from the indentation results highlighted the high sensitivity of the σ_Y and H to c_{Cr} and the low sensitivity of the B to c_{Cr} and c_{Co}.

Practical Ni-based alloys, such as U720Li, contain more than 10 additive elements that contribute to σ_Y and the strain-hardening behavior. Although this study focused only on ternary systems, the combinatorial testing and uniaxial property estimation represent valuable tools for investigating the mechanical properties of multi-component alloys and facilitate optimal alloy designs.

CRediT authorship contribution statement

Kenta Goto: Methodology, Investigation, Data curation, Writing – original draft. **Ayako Ikeda:** Methodology, Investigation, Data curation, Visualization. **Toshio Osada:** Conceptualization, Writing – review & editing, Project administration, Supervision. **Ikumu Watanabe:** Software, Resources. **Kyoko Kawagishi:** Resources, Supervision. **Takahito Ohmura:** Resources, Writing – review & editing, Supervision, Project administration, Funding acquisition.

Data Availability

The data required to reproduce these findings are available from the corresponding author upon request.

Declaration of Competing Interest

The authors declare that they have no known competing financial interests or personal relationships that could have appeared to influence the work reported in this paper.

Acknowledgments

This study was supported by the Innovative Science and Technology Initiative for Security, ATLA, Japan [Grant Number JPJ004596]. The authors appreciate Ms. Eri Nakagawa, Mr. Takuma Kohata, Mr. Masashi Hirosawa, Ms. Yuka Hara, Ms. Miwako Takano, and Mr. Kazuhiko Iida of National Institute for Materials Science for providing technical support. We would like to thank Editage (www.editage.com) for English language editing.

Appendix A. Supporting information

Supplementary data associated with this article can be found in the online version at doi:10.1016/j.jallcom.2022.164868.

References

[1] R.C. Reed, The Superalloys, Cambridge University Press, Cambridge, 2006.
[2] T. Osada, Y. Gu, N. Nagashima, Y. Yuan, T. Yokokawa, H. Harada, Optimum microstructure combination for maximizing tensile strength in a polycrystalline superalloy with a two-phase structure, Acta Mater. 61 (2013) 1820–1829, https://doi.org/10.1016/j.actamat.2012.12.004
[3] L. Wu, T. Osada, I. Watanabe, T. Yokokawa, T. Kobayashi, K. Kawagishi, Strength prediction of Ni-base disc superalloys: modified γ' hardening models applicable to commercial alloys, Mater. Sci. Eng. A 799 (2021) 140103, https://doi.org/10.1016/j.msea.2020.140103
[4] J.A. Yasi, L.G. Hector, D.R. Trinkle, First-principles data for solid-solution strengthening of magnesium: from geometry and chemistry to properties, Acta Mater. 58 (2010) 5704–5713, https://doi.org/10.1016/j.actamat.2010.06.045
[5] Z. Yang, J. Sun, S. Lu, L. Vitos, Assessing elastic property and solid-solution strengthening of binary Ni–Co, Ni–Cr, and ternary Ni–Co–Cr alloys from first-principles theory, J. Mater. Res. 33 (2018) 2763–2774, https://doi.org/10.1557/jmr.2018.174
[6] O. Franke, K. Durst, M. Göken, Nanoindentation investigations to study solid solution hardening in Ni-based diffusion couples, J. Mater. Res. 24 (2009) 1127–1134, https://doi.org/10.1557/jmr.2009.0135
[7] S.B. Kadambi, V.D. Divya, U. Ramamurty, Evaluation of solid-solution hardening in several binary alloy systems using diffusion couples combined with nanoindentation, Metall. Mater. Trans. A 48 (2017) 4574–4582, https://doi.org/10.1007/s11661-017-4250-3
[8] W. Li, L. Li, C. Wei, J. Zhao, Q. Feng, Effects of Ni, Cr and W on the microstructural stability of multicomponent CoNi-base superalloys studied using CALPHAD and diffusion-multiple approaches, J. Mater. Sci. Tech. 80 (2021) 139–149, https://doi.org/10.1016/j.jmst.2020.10.080
[9] W. Li, L. Li, S. Antonov, C. Wei, J. Zhao, Q. Feng, High-throughput exploration of alloying effects on the microstructural stability and properties of multi-component CoNi-base superalloys, J. Alloy. Compd. 881 (2021) 160618, https://doi.org/10.1016/j.jallcom.2021.160618
[10] A. Ikeda, K. Goto, T. Osada, I. Watanabe, K. Kawagishi, High-throughput mapping method for mechanical properties, oxidation resistance, and phase stability in Ni-based superalloys using composition-graded unidirectional solidified alloys, Scr. Mater. 193 (2021) 91–96, https://doi.org/10.1016/j.scriptamat.2020.10.043
[11] J. Ruzic, S. Emura, X. Ji, I. Watanabe, Mo segregation and distribution in Ti–Mo alloy investigated using nanoindentation, Mater. Sci. Eng. A 718 (2018) 48–55, https://doi.org/10.1016/j.msea.2018.01.098
[12] E. Gumbmann, F. De Geuser, A. Deschamps, W. Lefebvre, F. Robaut, C. Sigli, A combinatorial approach for studying the effect of Mg concentration on precipitation in an Al–Cu–Li alloy, Scr. Mater. 110 (2016) 44–47, https://doi.org/10.1016/j.scriptamat.2015.07.042
[13] H. Knoll, S. Ocylok, A. Weisheit, H. Springer, E. Jägle, D. Raabe, Combinatorial alloy design by laser additive manufacturing, Steel Res. Int. 88 (2017) 1600416, https://doi.org/10.1002/srin.201600416
[14] D.C. Hofmann, J. Kolodziejska, S. Roberts, R. Otis, R.P. Dillon, J.-O. Suh, Z.-K. Liu, J.-P. Borgonia, Compositionally graded metals: a new frontier of additive manufacturing, J. Mater. Res. 29 (2014) 1899–1910, https://doi.org/10.1557/jmr.2014.208
[15] K.L. Johnson, The correlation of indentation experiments, J. Mech. Phys. Solids 18 (1970) 115–126, https://doi.org/10.1016/0022-5096(70)90029-3
[16] R. Labusch, A statistical theory of solid solution hardening, Phys. Status Solidi 41 (1970) 659–669, https://doi.org/10.1002/pssb.19700410221
[17] J.M. Rickman, H.M. Chan, M.P. Harmer, J.A. Smeltzer, C.J. Marvel, A. Roy, G. Balasubramanian, Materials informatics for the screening of multi-principal elements and high-entropy alloys, Nat. Commun. 10 (2019) 1–10, https://doi.org/10.1038/s41467-019-10533-1
[18] P. Wilson, R. Field, M. Kaufman, The use of diffusion multiples to examine the compositional dependence of phase stability and hardness of the Co-Cr-Fe-Mn-Ni high entropy alloy system, Intermetallics 75 (2016) 15–24, https://doi.org/10.1016/j.intermet.2016.04.007
[19] A.G. Atkins, D. Tabor, Plastic indentation in metals with cones, J. Mech. Phys. Solids 13 (1965) 149–164, https://doi.org/10.1016/0022-5096(65)90018-9
[20] I. Watanabe, Z. Sun, H. Kitano, K. Goto, Multiscale analysis of mechanical behavior of multilayer steel structures fabricated by wire and arc additive manufacturing, Sci. Technol. Adv. Mater. 21 (2020) 461–470, https://doi.org/10.1080/14686996.2020.1788908
[21] T.-H. Pham, Q.-M. Phan, S.-E. Kim, Identification of the plastic properties of structural steel using spherical indentation, Mater. Sci. Eng. A 711 (2018) 44–61, https://doi.org/10.1016/j.msea.2017.10.097
[22] H. Chen, L. Cai, Theoretical model for predicting uniaxial stress-strain relation by dual conical indentation based on equivalent energy principle, Acta Mater. 121 (2016) 181–189, https://doi.org/10.1016/j.actamat.2016.09.008

[23] M. Kim, J.H. Lee, F. Rickhey, H. Lee, A dual triangular pyramidal indentation technique for material property evaluation, J. Mater. Res. 30 (2015) 1098–1109, https://doi.org/10.1557/jmr.2015.67
[24] K. Goto, I. Watanabe, T. Ohmura, Sensitivity analysis of indentation and inverse estimation of elastoplastic property, Proc. Mater. Mech. Conf., 2018, p. OS0903. ⟨https://doi.org/10.1299/jsmemm.2018.OS0903⟩.
[25] K. Goto, I. Watanabe, T. Ohmura, Inverse estimation approach for elastoplastic properties using the load-displacement curve and pile-up topography of a single Berkovich indentation, Mater. Des. 194 (2020) 108925, https://doi.org/10.1016/j.matdes.2020.108925
[26] J.O. Andersson, T. Helander, L. Höglund, P. Shi, B. Sundman, Thermo-calc & DICTRA, computational tools for materials science, Calphad Comput, Coupling Phase Diagr. Thermochem 26 (2002) 273–312, https://doi.org/10.1016/S0364-5916(02)00037-8
[27] W.C. Oliver, G.M. Pharr, An improved technique for determining hardness and elastic modulus using load and displacement sensing indentation experiments, J. Mater. Res. 7 (1992) 1564–1583, https://doi.org/10.1557/JMR.1992.1564
[28] E.D. Hintsala, U. Hangen, D.D. Stauffer, High-throughput nanoindentation for statistical and spatial property determination, JOM 70 (2018) 494–503, https://doi.org/10.1007/s11837-018-2752-0
[29] T. Nishizawa, K. Ishida, The Co-Ni (Cobalt-Nickel) system, Bull. Alloy Phase Diagr. 4 (1983) 390–395, https://doi.org/10.1007/BF02868090
[30] G. Bracq, M. Laurent-Brocq, L. Perrière, R. Pirès, J.M. Joubert, I. Guillot, The fcc solid solution stability in the Co-Cr-Fe-Mn-Ni multi-component system, Acta Mater. 128 (2017) 327–336, https://doi.org/10.1016/j.actamat.2017.02.017
[31] J.J. Vlassak, W.D. Nix, Measuring the elastic properties of anisotropic materials by means of indentation experiments, J. Mech. Phys. Solids 42 (1994) 1223–1245.
[32] E. Renner, Y. Gaillard, F. Richard, F. Amiot, P. Delobelle, Sensitivity of the residual topography to single crystal plasticity parameters in Berkovich nanoindentation on FCC nickel, Int. J. Plast. 77 (2016) 118–140, https://doi.org/10.1016/j.ijplas.2015.10.002
[33] T.B. Britton, H. Liang, F.P.E. Dunne, A.J. Wilkinson, The effect of crystal orientation on the indentation response of commercially pure titanium: experiments and simulations, Proc. R. Soc. A Math. Phys. Eng. Sci. 466, 2010, pp. 695–719. ⟨https://doi.org/10.1098/rspa.2009.0455⟩.
[34] V. Petley, S. Sathishkumar, K.H. Thulasi Raman, G.M. Rao, U. Chandrasekhar, Microstructural and mechanical characteristics of Ni-Cr thin films, Mater. Res. Bull. 66 (2015) 59–64, https://doi.org/10.1016/j.materresbull.2015.02.002
[35] K. Goto, I. Watanabe, T. Ohmura, Determining suitable parameters for inverse estimation of plastic properties based on indentation marks, Int. J. Plast. 116 (2019) 81–90, https://doi.org/10.1016/j.ijplas.2018.12.007
[36] K. Durst, B. Backes, M. Göken, Indentation size effect in metallic materials: correcting for the size of the plastic zone, Scr. Mater. 52 (2005) 1093–1097, https://doi.org/10.1016/j.scriptamat.2005.02.009
[37] L.A. Gypen, A. Deruyttere, Multi-component solid solution hardening, J. Mater. Sci. 12 (1977) 1028–1033, https://doi.org/10.1007/BF00540987
[38] C. Varvenne, A. Luque, W.A. Curtin, Theory of strengthening in fcc high entropy alloys, Acta Mater. 118 (2016) 164–176, https://doi.org/10.1016/j.actamat.2016.07.040
[39] H.A. Roth, C.L. Davis, R.C. Thomson, Modeling solid solution strengthening in nickel alloys, Metall. Mater. Trans. A 28 (1997) 1329–1335, https://doi.org/10.1007/s11661-997-0268-2
[40] A. Akhtar, E. Teghtsoonian, Plastic deformation of Ni-Cr single crystals, Metall. Trans. 2 (1971) 2757–2763, https://doi.org/10.1007/BF02813249
[41] S. Yoshida, T. Ikeuchi, Y. Bai, N. Tsuji, Effect of cobalt-content on mechanical properties of non-equiatomic Co–Cr–Ni medium entropy alloys, Mater. Trans. 61 (2020) 587–595, https://doi.org/10.2320/matertrans.MT-MK2019004